ISSN: 0067-2904

CdO: SnO_2 Composite UV-Assisted Room Temperature Ozone Sensor

Mohammed O. Salman[1*], Mohammed A.Kadhim [2], Abed A. Khalefa [3]
[1]*Department of Medical Physics, College of Applied Science, University of Fallujah, Iraq*
[2]*University of Kerbala College of Science*
[3]*Ministry of Education, General Directorate of Salah AL-din*

Received: 30/9/2021 Accepted: 20/7/2022 Published: 30/3/2023

Abstract

Cadmium-tin oxide (CSO) thin films were fabricated by spray pyrolysis method at different substrate temperatures (T_s). The results showed a significant effect of T_s on the surface morphology and the electrical properties, which in turn has a significant effect on sensor gas sensitivity. The sample prepared at 400 °C appeared in the form of a donut shape, which has the best ozone sensitivity. No ozone sensitivity appeared in-dark, while showed good sensitivity when illuminated with UV at room temperature (RT). The study showed that the photon exposure method can substitute for the conventional method of sensors heating.

Keywords: Metal oxide, Cd–Sn oxide, gas sensor, UV-assisted sensor, Ozone sensor.

مستشعر الأوزون للمركب CdO: SnO_2 في درجة حرارة الغرفة بمساعدة الأشعة فوق البنفسجية

محمد عودة سلمان [1 *]، محمد عبد الحر كاظم [2]، عبد أحمد خليفة[3]

[1] قسم الفيزياء الطبية، كلية العلوم التطبيقية ، جامعة الفلوجة، العراق

[2] كلية العلوم، جامعة كربلاء

[3] وزارة التربية والتعليم، المديرية التربية العامة في صلاح الدين

الخلاصة

تم تصنيع الأغشية الرقيقة من أكسيد الكادميوم – القصدير (CSO) عن طريق الانحلال الحراري بالرش عند درجات حرارة مختلفة (T_s). أظهرت النتائج تأثيرا كبير لدرجة حرارة الأرضية على شكل السطح والخواص الكهربائية والتي بدورها لها تأثير كبير على حساسية الغاز. ظهرت العينة المحضرة عند درجة حرارة 400 درجة مئوية على شكل دونات ، والتي لها أفضل حساسية للأوزون. لم تظهر أي حساسية للأوزون في الظلام ، بينما أظهرت حساسية جيدة عند الإضاءة بالأشعة فوق البنفسجية في درجة حرارة الغرفة (RT). أظهرت الدراسة أن طريقة التعرض للفوتون يمكن أن تحل محل الطرق التقليدية بتسخين أجهزة الاستشعار.

* Email: dr.mohammedodehsalman@uofallujah.edu.iq

1. Introduction

Ozone is a strong oxidizing agent used in many aspects of a person's life for sanitization and purification. Furthermore, it is a toxic gas that is very harmful to health. Ozone is produced when NO_2 polluted air is exposed to sunlight. In the natural environment, the ozone concentration is around 30 parts per billion. It is essential to monitor ozone concentrations to maintain human health [1]. Metal oxides are good candidates for sensor applications. The physical properties of metal oxides thin-film, such as electrical behaviour, depend highly on oxygen vacancies [2] and point defects [3]. Usually, gas sensors do not work or are of low sensitivity at room temperature(RT) but operate at higher temperatures. The sensors need a heater to activate the reactions on the surface of the active substance [4], [5].

Many studies have been conducted to reduce the temperature at which the sensor operates by using a large variety of nanostructures [6] in the form of nanoparticles [7], nanotubes [8], nanobelts [9] etc., which are prepared by various techniques including hydrothermal [10], electrospinning [11], sol-gel [12], thermal evaporation [4], etc. Also, RT gas sensor sensitivity can be enhanced using ultraviolet radiation (UV) [1]. Many experimental studies have stated the sensing mechanism of UV-assisted gas sensors [13]. The detection mechanism depends on the fact that some metal oxides have good sensitivity to some types of gases, and also possess photocatalytic properties. The electron-hole pairs created by light contribute to enhancing the chemical reactions between the gas molecules and the anions adsorbed on the metal oxide surface [14].

In this paper, the possibility of obtaining ternary phase $CdSnO_3$ using simple spray pyrolysis method using the stoichiometric ionic ratio Cd/Sn was studied. The structural and electrical behaviour of deposited samples at different substrate temperature (T_s) were investigated. Finally, the effect of UV-radiation on ozone sensing at RT for the films deposited at different T_s was investigated.

2. Experimental

Cadmium-tin oxide(CSO) films were deposited on glass slides by the spray pyrolysis method. Tin(II) chloride dihydrate ($SnCl_2$:$2H_2O$) of purity ≥ 99 % (Sigma-Aldrich Co.)and cadmium chloride ($CdCl_2$) of purity ≥99 % (Sigma-Aldrich Co.) at Sn: Cd (1:1) ionic ratio were dissolved in 1:1 alcohol to distilled water solution . The weights of powders were mixed with the specific molar ratio and dissolved in liquid at 0.1 M by stirring at RT until all the added powder was dissolved. In the spray pyrolysis system, the atomizer was positioned at 30 cm away from the glass substrates which were placed on a hot plate heater of controlled temperature. 10 ml of the prepared solution was sprayed onto the glass substrates at a spray rate of 2 ml/min. The spray was intermittent, open for 10 seconds and closed for 5 seconds, using a controlled valve that closes the way of the compressed air at a pressure of five bar. The thin films were deposited at different substrate temperature T_s of 300, 400, and 500 °C.

The prepared thin films were studied by X-ray diffraction, FE-SEM and Hall effect measurements.

To fabricate the gas sensor, aluminium electrodes were deposited by thermal evaporation as a comb-like pattern on the sample's surface of dimensions as shown in Figure 1.

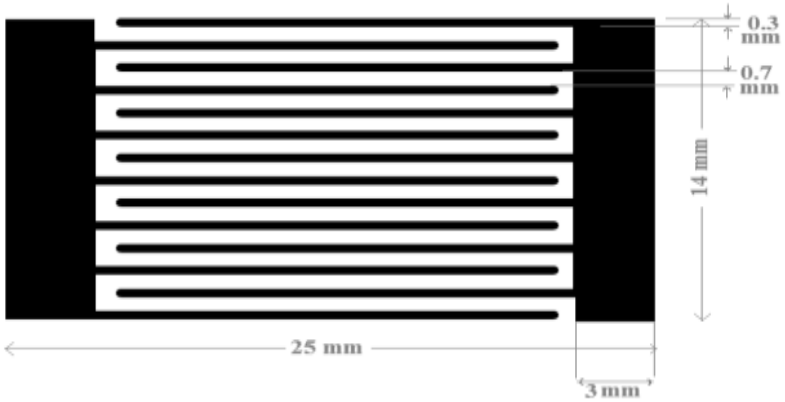

Figure 1: Electrodes dimensions for the gas sensor.

The fabricated ozone sensor was examined at RT in a homemade sealed cylindrical chamber with a diameter of 5 cm and a height of 5 cm. The ozone sensitivity was examined using the flow-through technique (at a constant flow of 0.5 ml/min) with the exposure of the sensor to UV light of around 300 nm wavelength to create photo-generated electron-hole pairs. The LED-sensor separation distance was fixed at 2 cm for all tests. Ozone was supplied from an ozone generator and mixed with dry air using a flowmeter. The fabricated sensor was exposed to the ozone-air mixture, and at the same time, detected by a handled ozone monitor. The resistance variation of the sensor was measured when the sample was exposed to the ozone-air mixture and turned off, using a multimeter connected with a computer as shown in the schematic diagram of Figure 2.

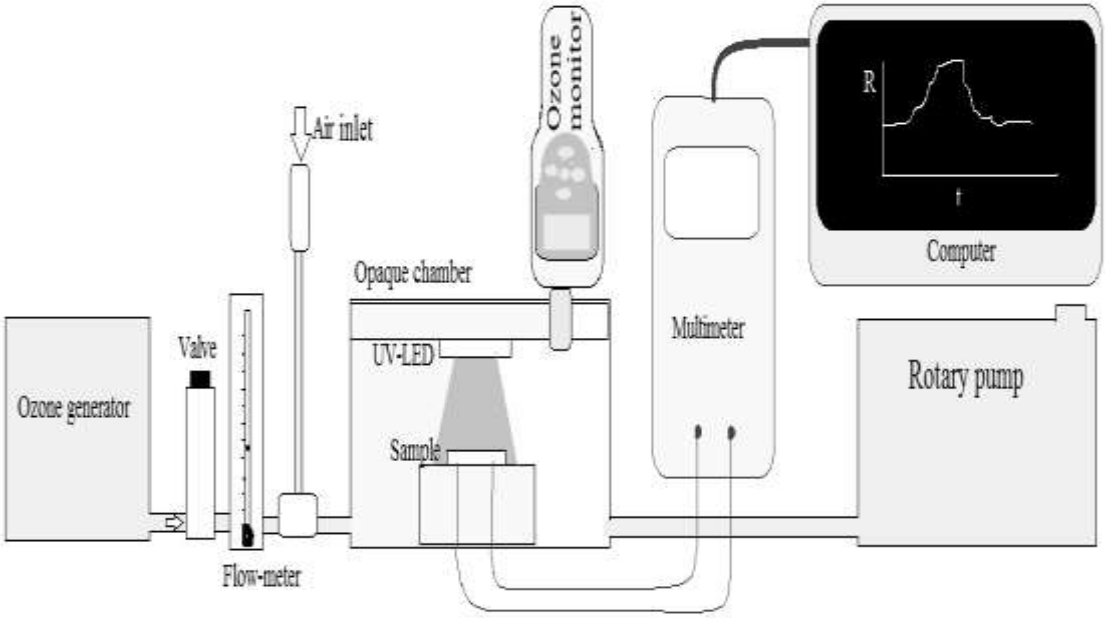

Figure 2: Schematic diagram of UV-assisted ozone sensor examination.

3. Results and Discussions

Figure 3 shows the XRD patterns for the prepared CSO thin films on glass slides at different temperatures*(T_s)*300, 400, and 500 °C. Polycrystalline structure of mixed phases appeared in the three samples, matched with SnO_2 tetragonal crystal structure, CdO cubic structure, and an additional minor phase of $CdSnO_3$ appearing at the highest temperature, corresponding to the JCPDS file numbers 41-1445, 75-0594, and 34-0758, respectively. The

peaks width (FWHM) decreased with increasing the deposition temperature indicating an increase of the crystalline size (C.S), as shown by Scherrer's equation [15]:

$$C.S = \frac{0.9\,\lambda}{FWHM\,.cos(\theta)} \qquad \text{……..(1)}$$

Where: λ, θ, and FWHM are the monochromatic X-ray wavelength (λ =1.5406 Å), diffraction angle and full width at half maximum of the diffraction lines. The FWHM for the peaks was measured by Lorentzian fitting using XPowder software.

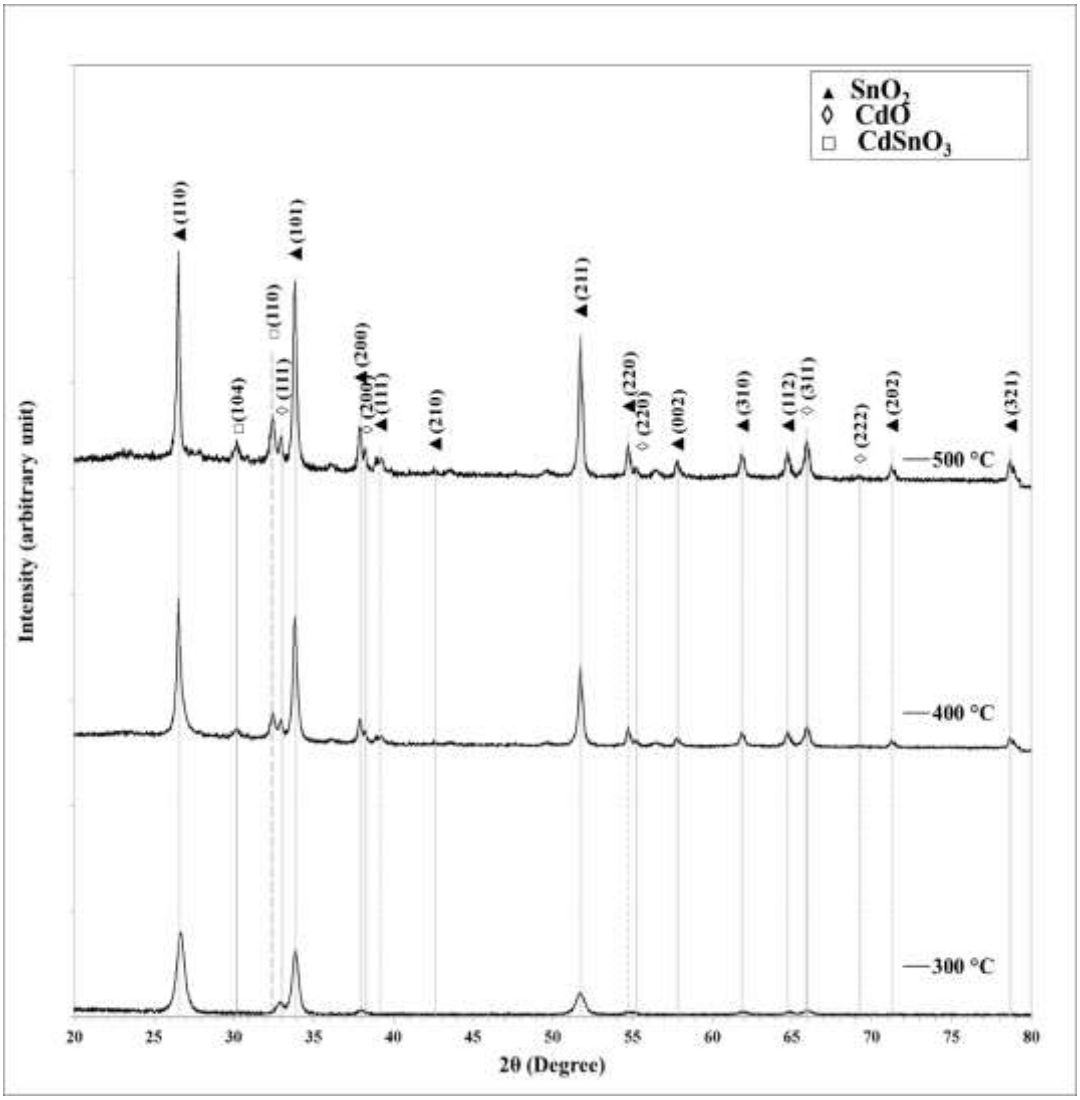

Figure 3: XRD patterns for SnO_2:CdO thin films deposited at different substrates temperatures.

The inter-Planar spacing (d_{hkl}) was calculated by Bragg's formula : [16]

$$n\,\lambda = 2\,d_{hkl}\,sin\,\theta \qquad \text{……(2)}$$

where *n* is the diffraction order.

Table 1 displays the diffraction peaks parameters including 2θ, FWHM, d_{hkl}, crystallite size (C.S.) and corresponding Miller indices for the thin films prepared at different T_s. It appears that the calculated crystallite size decreased with increasing T_s.

Table 1: XRD peaks parameters for CSO thin films prepared at different substrate temperatures

T_s (°C)	2θ (Deg.)	FWHM (Deg.)	d_{hkl} Exp. (Å)	C.S (nm)	Phase	hkl
300	26.6809	0.5782	3.3384	14.1	TetragonalSnO_2	(110)
	32.9122	0.4994	2.7192	16.6	Cubic CdO	(111)
	33.8758	0.4424	2.6440	18.8	TetragonalSnO_2	(101)
	37.9872	0.4800	2.3668	17.5	TetragonalSnO_2	(200)
	51.7345	0.6351	1.7656	13.9	TetragonalSnO_2	(211)
	54.8822	0.6700	1.6715	13.4	TetragonalSnO_2	(220)
	61.9486	0.6540	1.4967	14.2	TetragonalSnO_2	(310)
	64.8394	0.5700	1.4368	16.5	TetragonalSnO_2	(112)
	65.9957	0.6500	1.4144	14.6	Cubic CdO	(311)
400	26.5468	0.3597	3.3550	22.7	TetragonalSnO_2	(110)
	30.2158	0.4316	2.9554	19.1	$CdSnO_3$	(104)
	32.4460	0.3597	2.7572	23.0	$CdSnO_3$	(110)
	32.9496	0.2518	2.7162	32.9	Cubic CdO	(111)
	33.8489	0.3597	2.6461	23.1	TetragonalSnO_2	(101)
	37.9137	0.2877	2.3712	29.2	TetragonalSnO_2	(200)
	39.1367	0.5396	2.2999	15.6	TetragonalSnO_2	(111)
	51.7266	0.3957	1.7658	22.3	TetragonalSnO_2	(211)
	54.7122	0.3597	1.6763	24.9	TetragonalSnO_2	(220)
	55.2518	0.2878	1.6612	31.2	Cubic CdO	(202)
	57.8417	0.5036	1.5928	18.0	TetragonalSnO_2	(002)
	61.8345	0.3597	1.4992	25.7	TetragonalSnO_2	(310)
	64.7482	0.3598	1.4386	26.1	TetragonalSnO_2	(112)
	65.9712	0.4676	1.4149	20.3	Cubic CdO	(311)
	71.2590	0.3957	1.3223	24.7	TetragonalSnO_2	(202)
	78.7050	0.5396	1.2148	19.0	TetragonalSnO_2	(321)
500	26.5468	0.2877	3.3550	28.4	TetragonalSnO_2	(110)
	30.1799	0.4677	2.9589	17.6	$CdSnO_3$	(104)
	32.4460	0.3597	2.7572	23.0	$CdSnO_3$	(110)
	32.9856	0.2518	2.7133	32.9	Cubic CdO	(111)
	33.8489	0.2878	2.6461	28.9	TetragonalSnO_2	(101)
	37.9137	0.2518	2.3712	33.4	TetragonalSnO_2	(200)
	38.3094	0.2158	2.3476	39.0	Cubic CdO	(200)
	39.0288	0.5396	2.3060	15.6	TetragonalSnO_2	(111)
	51.7626	0.3237	1.7647	27.3	TetragonalSnO_2	(211)
	54.7122	0.2878	1.6763	31.1	TetragonalSnO_2	(220)
	57.8058	0.3237	1.5937	28.0	TetragonalSnO_2	(002)
	61.8345	0.3597	1.4992	25.7	TetragonalSnO_2	(310)
	64.7482	0.3598	1.4386	26.1	TetragonalSnO_2	(112)
	65.9712	0.4317	1.4149	21.9	Cubic CdO	(311)
	71.3309	0.3957	1.3212	24.7	TetragonalSnO_2	(202)
	78.7050	0.4676	1.2148	22.0	TetragonalSnO_2	(321)

The surface morphology of the CSO thin films deposited at different T_s was examined using FE-SEM. Figure 4 shows the FE-SEM images, at two magnification powers, for the CSO sample prepared at a T_s of 300 °C. The images show clusters, of diameters around 300 nm, composed of small spherical particles of diameter between (63 – 85) nm, highly connected to each other.

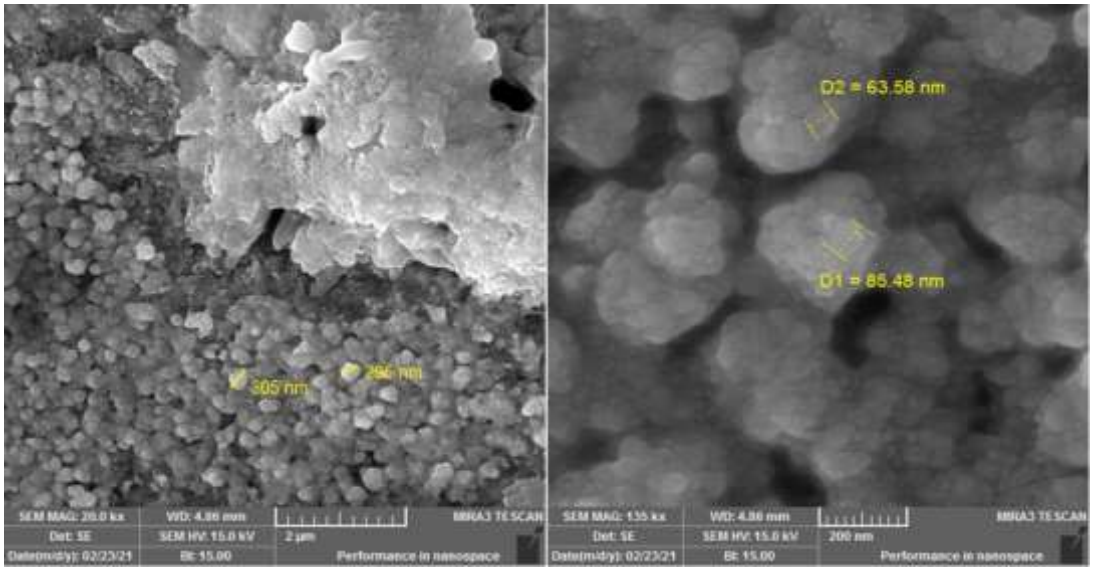

Figure 4: FE-SEM images at two magnifications for CdO:SnO_2 thin films prepared at 300 °C T_s

The sample prepared at 400 °C appeared in the form of a donut shape with a diameter of approximately 500 nm, consisting of small particles with a diameter of (47 to 81) nm compacted together. These nanoscale shapes were randomly distributed on the surface separated by spaces. Such an arrangement possesses large effective surface area that can interact with the surrounding gas molecules, which enhances the gas sensitivity properties, as great surface area to bulk ratio. The charge carrier depletion layer, that usually forms near the surfaces [17], decreases the concentration of charge carriers, causing a significant change in the sample conductance when interacting with the target gas. There are many studies that have shown the possibility of preparing pure and doped tin oxide with different nanostructures. Umar reported, for the first time, the formation of donut-shaped crystalline SnO_2 structures[18].

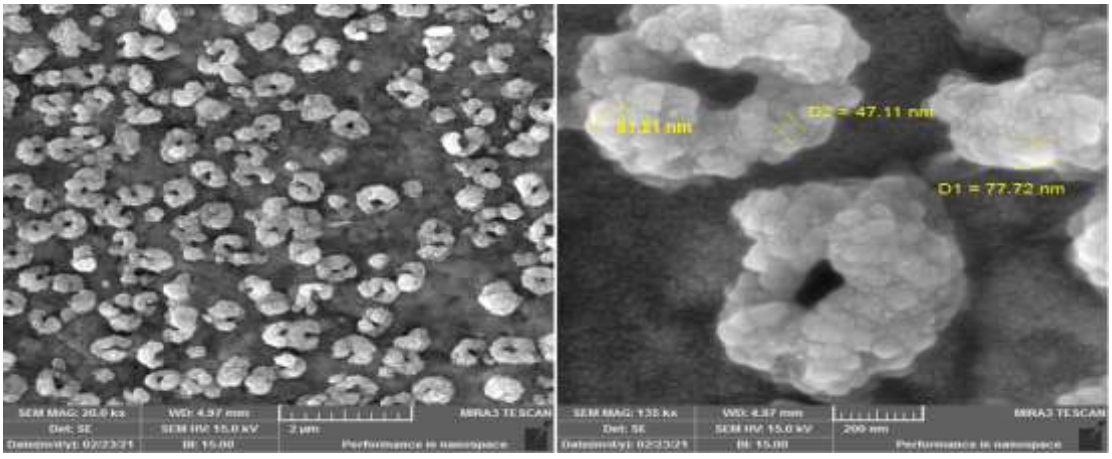

Figure 5: FESEM images at two magnifications for CdO:SnO_2 deposited at 400 °C T_s

The sample prepared at 500 °C appeared as adherent flakes, with a diameter of up to 300 nm, randomly distributed on sample surface. This sample has less surface area than the previous sample. The FE-SEM examinations showed a significant variation in the topography of the prepared samples, which affected the gas sensing [19]. The deposition temperature has a high effect on the final nanostructure shapes due to variation of growth mechanism with temperature [20].

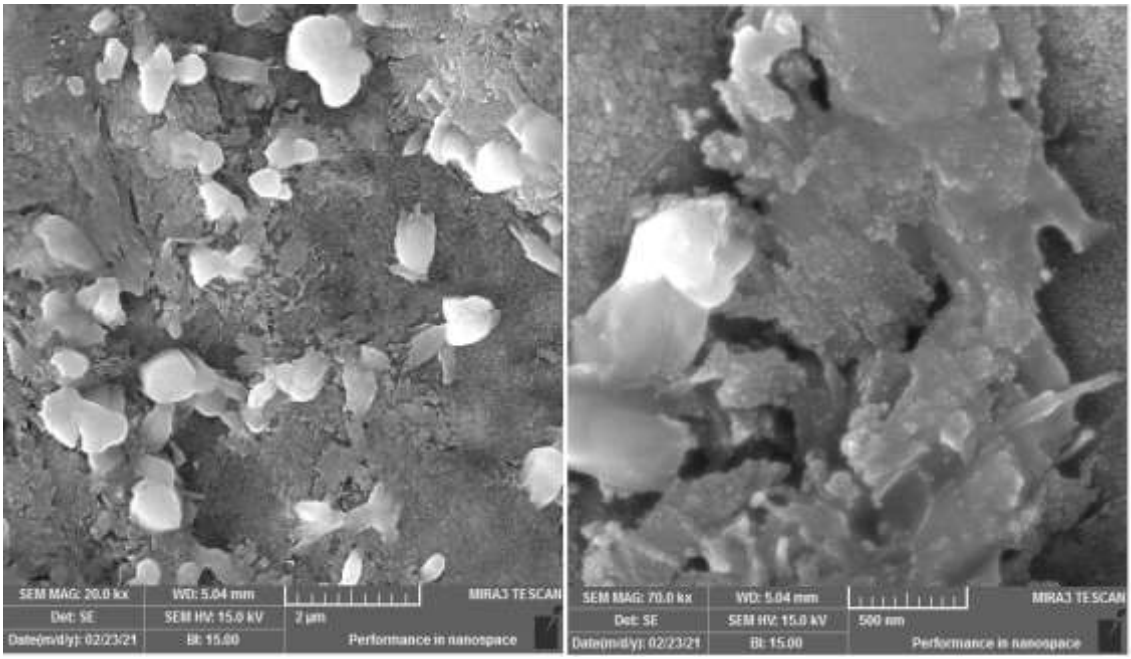

Figure 6: FESEM images at two magnifications for CdO:SnO_2 thin films deposited at 500 °C

After deposition, appropriate aluminium electrodes were deposited on the sample by thermal evaporation. Hall Effect measurements, including Hall coefficient (R_H), carrier concentration (N_H), Hall mobility (μ_H), and conductivity (σ), were done to determine the electrical properties for the CSO thin films at different T_s, as shown in Table 2. All films were proved to be n-type semiconductor due to oxygen vacancies. Usually, the presence of oxygen vacancies in some wide bandgap metal oxides, such as SnO_2, cause it to behave as n-type semiconductor [21].

Table 2: Hall parameters for the CdO:SnO_2 thin films prepared at different T_s

T_s (°C)	$\sigma(\Omega\ cm)^{-1} \times 10^{-4}$	R_H (cm^3/C) $\times 10^5$	$N_H\ cm^{-3} \times 10^{13}$	$\mu_H\ cm^2$/V.s	Type
300	4.2	-3.20	1.953	134	n
400	6.3	-2.54	2.461	160	n
500	10	-2.71	2.306	271	n

The variation of σ, N_H and μ_H with T_s are shown in Figure 7. It appears that T_s highly affects the electrical behaviour of the CdO:SnO_2 composite film. The conductivity increased from 4.2×10^{-4} to 1×10^{-3} $\Omega^{-1}.cm^{-1}$ with increasing the temperature from 300 to 500 °C. The increment in conductivity can be explained by the increase of crystallite size with increasing T_s, thus reducing the grain boundary scattering and increasing conductivity due to increased carrier mobility. The carrier concentration increased as T_s increased from 300 to 400 °C. This increase in carrier concentration may be due to an increase in the diffusion of Sn atoms into CdO lattice, which acts as donors due to the Sn atom valence of 4, and 2 for the Cd atom. Hence, the increase of electron concentration with increasing T_s. At high T_s, the carrier

concentration was found to decrease, may be due to a decrease in oxygen vacancies with improving crystallinity [22].

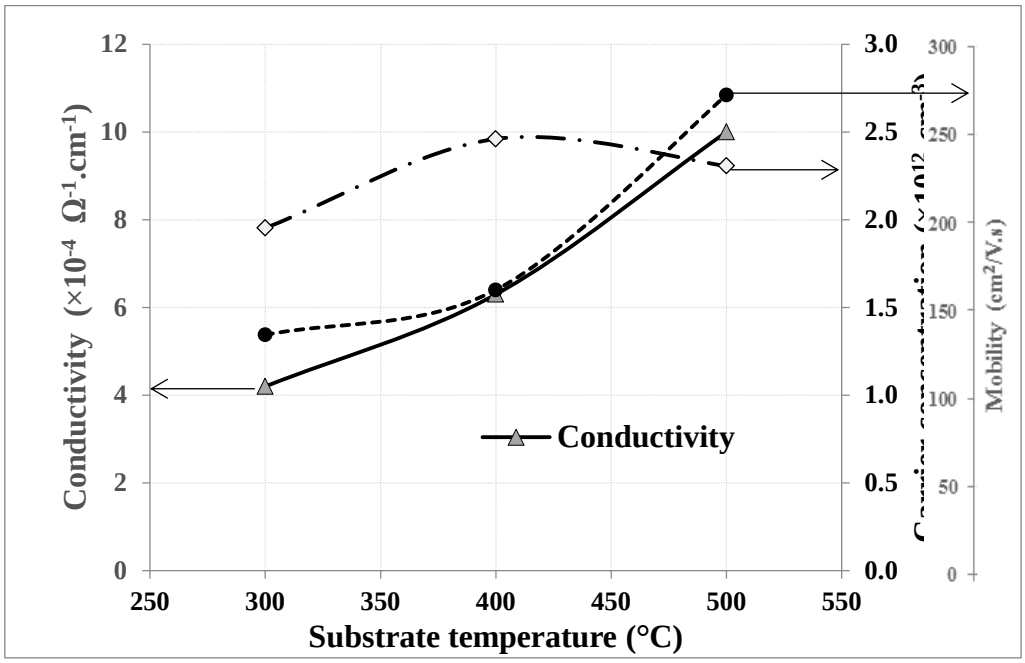

Figure 7: Changes of N_H, μ_H and σ with T_s

The sensitivity of the sensor samples, deposited at different temperatures, to ozone gas as well as to other gases (NO_2 and NH_3) was tested at RT without exposure to the UV, the sensor showed no sensitivity to the gasses. The sensor samples showed good sensitivity to ozone with the presence of an ultraviolet source at RT. Figure 8 illustrates the resistance fluctuation of CdO:SnO_2 composite thin films sensor, prepared at 400 °C when the samples were cyclic exposed to ozone gas and clean air successively. The figure shows a good stability of the sensor at multiple cycles, with close values of resistance change for the same concentration (5 ppm).

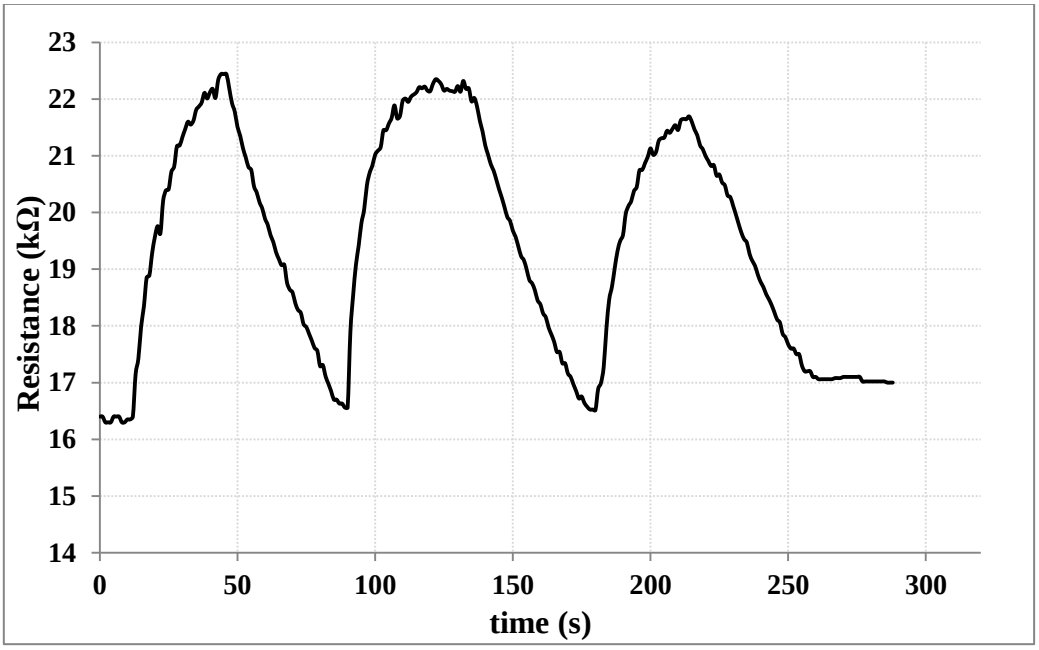

Figure 8: Resistance variation with time for the CdO:SnO_2 thin film sensor sample prepared at 400 °C when exposed to 5 ppm ozone concentrations with UV exposure.

Figure 9 shows the resistance variation with time for SnO_2:CdO sensor samples prepared at different temperatures, at different ozone concentrations, at room temperature with UV exposure. The resistance was found to increase with different values of gas exposure which is proportional to the ozone concentration. The sensor sample prepared at 400 °C appeared to have better sensitivity than the other two samples because of its large surface area.

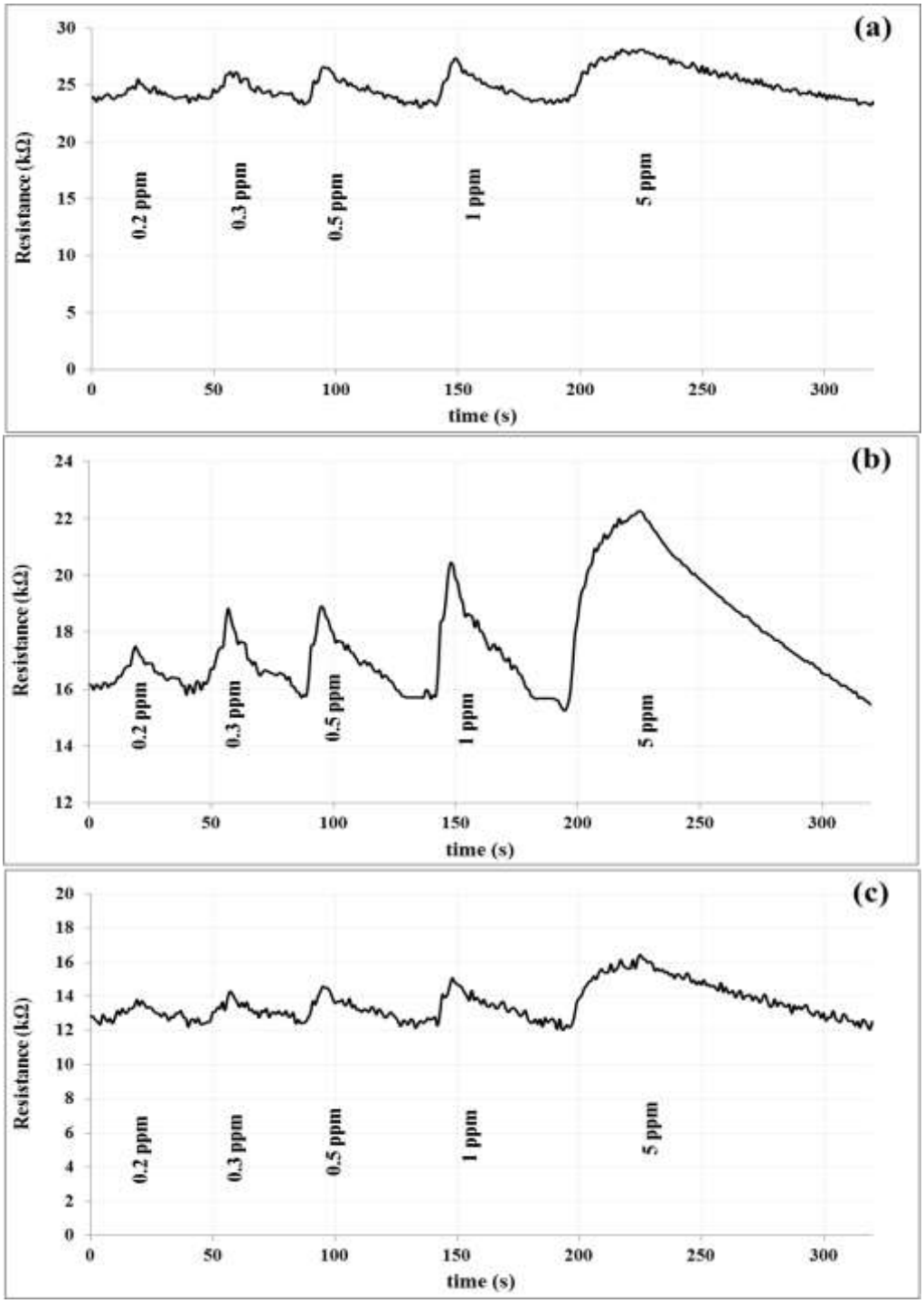

Figure 9: Resistance variation with time for SnO_2:CdO thin film sensor samples prepared at (a) 300 °C, (a) 400 °C, and (a) 500 °C when exposed to different ozone concentrations with UV-exposure.

Figure 10 illustrates the sensitivity of the SnO_2:CdO sensor, based on CSO films deposited at different T_s , as a function of ozon concentration assisted by UV light exposure at RT. The sensitivity was found to increase with gas concentration in an exponential manner as the equations of $y = 10.684x^{0.3164}$, $y = 16.834x^{0.4419}$, and $y = 26.542x^{0.3953}$ for the samples prepared at 300, 400, and 500 °C T_s, respectively. The fitting lines have an acceptable value of R^2 (greater than 0.9).

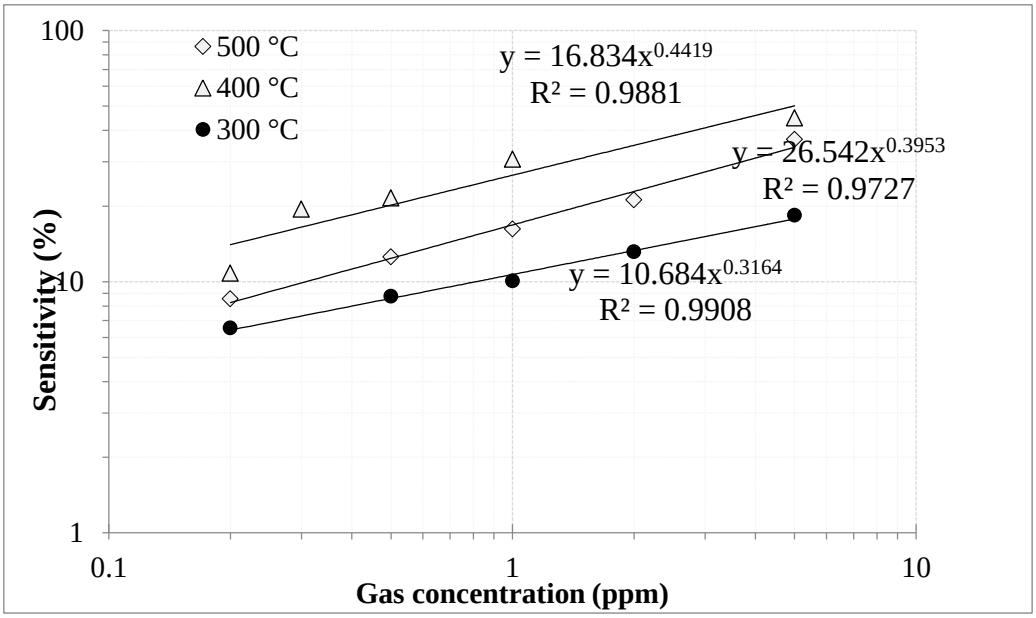

Figure 10: Variation of sensitivity with gas concentration for samples prepared at different T_s

The response and recovery times are distinct as the required period for the sensor to reach 90% of the total signal change when exposed to ozone with UV exposure, and when return to 10% of the original baseline after ozone flow closed, respectively, as shown in Figure 11.

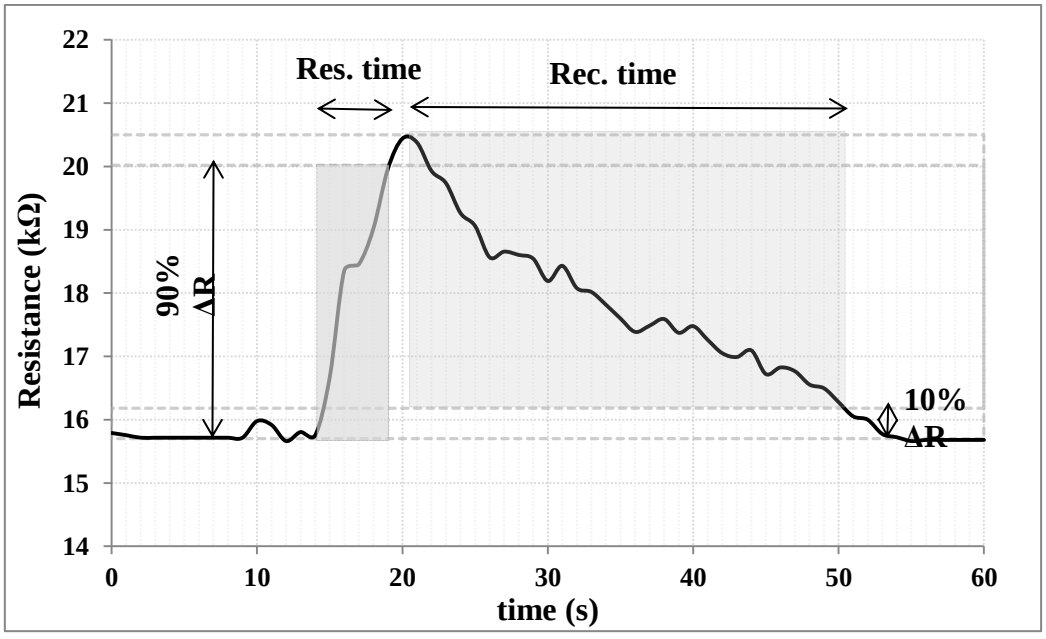

Figure11: The response time (5 s) and recovery time (30 s) for the UV assisted-SnO_2:CdO sensor prepared at 300°C when exposed to 2 ppm ozone at RT.

Figure 12 shows the variation of response and recovery times for the sensor prepared at 300 °C T_s with UV assistance at RT, with the change of the gas concentration. The period of response was shorter than the recovery at all concentrations, which means that traps and other defects are involved in the process.

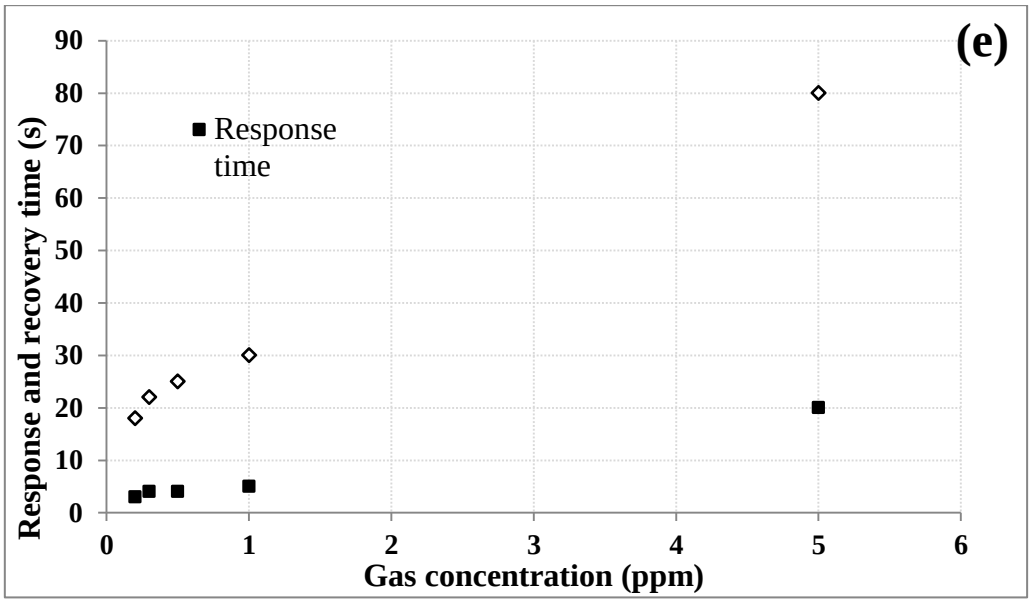

Figure 12: Variation of response time and recovery time for the UV assisted-SnO_2:CdO sensor prepared at 300°C with ozone concentration at RT.

The mechanism of ozone sensing with the UV-assistance can be clarified as: First, the surface of the active layer exposed to air adsorbed oxygen molecules, which will capture the electrons from the conduction band, causing the formation of depletion layer at the sample surface and oxygen anions on the surface. The dominant species at RT is O_2^- which is adsorbed from ambient oxygen [17]. The O_2^- anion on the sensor surface can be considered thermally stable at RT, so it is non-reactive in dark conditions owing to its high absorption energy. The sensitivity is improved by UV illumination as the exposed samples to ultraviolet radiation generates hole-electron pairs, followed by migration of the holes to the sample surface that interacts with the O^{-2} and desorbs these from the sample surface as the reaction ($h^+ + O_2^-$ ads $\rightarrow O_2$) [23] forming an active surface. The adsorbed O_3 on the surface and grain boundaries act as traps for photo-excited electrons, causing the increase in the potential barrier height at grain boundaries; therefore, the resistivity increases [24]. The mechanism of photo-assisted sensitivity for metal oxides to ozone gas has been explained in many studies [25, 26].

4. Conclusions

A room temperature UV-assisted ozone sensor was fabricated from cadmium-tin oxide (CSO) thin films by a low-cost spray pyrolysis technique. The structural measurements, surface topography and electrical properties were significantly affected by the deposition temperature. The deposition temperature changed the nanostructure shapes, their crystallinity and the charge carrier density, which affected their gas sensitivity.

The prepared samples show no response to ozone under dark condition, while showing good sensitivity to ozone when exposed to ultraviolet light at RT. The resistance fluctuation for the CSO thin films showed good stability of the sensor, and the best sensitivity appeared for the sample prepared at 400 °C T_s. The sensitivity varied according to surface morphology,

where the best samples appeared at 400°C T_s due to the novel shape of donut nanoparticles. The UV source generated free charge carriers, which made the samples sensitive to ozone gas. This means that the photon exposure method can substitute the conventional method of heating the sensors. The results were promising to realize a good specification ozone sensor operating at RT.

5. References

[1] J.H. Yu, H.J. Yang, H.S. Mo, T.S. Kim, T.S. Jeong, C. J. Youn & K. J. Hong, "Sensing Mechanism and Behavior of Sputtered ZnCdO Ozone Sensors Enhanced by Photons for Room-Temperature Operation," *J. Electron. Mater.*, vol. 42, no. 4, pp. 720–725, 2013, doi: 10.1007/s11664-012-2462-2.

[2] W. Jung, S. H. Lee, S. Y. Park, E. Lee, J. Bae, N. Park, J. Kim, and C. Jeon, "Electrical and Optical Properties of Cd 2 SnO 4 Thin Film Depending on its Chemical Bond," *Mol. Cryst. Liq. Cryst.*, vol. 551, no. 1, pp. 123–129, 2011, doi: 10.1080/15421406.2011.600628.

[3] T Stapinski, E Leja and T Pisarkiewicz,"Point defects and their influence on electrical properties of reactive sputtered Cd_2SnO_4 thin films," *J.Phys. D: Appl. Phys.*, vol. 17, no. 2, pp. 407–413, 1984, doi: https://doi.org/10.1088/0022-3727/17/2/025.

[4] Z. Q. Zheng, L. F. Zhu, and B. Wang, "In_2O_3 Nanotower Hydrogen Gas Sensors Based on Both Schottky Junction and Thermoelectronic Emission," *Nanoscale Res. Lett.*, vol. 10, article no.:293, 2015, doi: 10.1186/s11671-015-1002-4.

[5] Z. Li, Q. Zhao, W. Fan, and J. Zhan, "Porous SnO2 nanospheres as sensitive gas sensors for volatile organic compounds detection," *Nanoscale*, vol. 3, no. 4, pp. 1646–1652, 2011, doi: 10.1039/c0nr00728e.

[6] M. M. Arafat, B. Dinan, S. A. Akbar, and A. S. M. A. Haseeb, "Gas Sensors Based on One Dimensional Nanostructured Metal-Oxides: A Review," *Sensors(Basel)*, vol. 12, no. 6, pp. 7207–7258, 2012, doi: 10.3390/s120607207.

[7] A. M. Alwan, A. A. Yousif, and H. R. Abed, "High sensitivity and fast response at the room temperature of SnO2:CuO/PSi nanostructures sandwich configuration NH3 gas sensor," *AIP Conference Proceedings*, vol. 2190 , no.1, p. 020086, 2019, doi: 10.1063/1.5138572.

[8] B. Y. Wei, M. C. Hsu, P. G. Su, H. M. Lin, R. J. Wu, and H. J. Lai, "A novel SnO2 gas sensor doped with carbon nanotubes operating at room temperature," *Sensors and Actuators B: Chemical*, vol. 101, no. 1–2, pp. 81–89, 2004, doi: 10.1016/j.snb.2004.02.028.

[9] P. H. Suman, A. A. Felix, H. L. Tuller, J. A. Varela, and M. O. Orlandi, "Comparative gas sensor response of SnO2 , SnO and Sn3O4 nanobelts to NO2 and potential interferents," *Sensors and Actuators B: Chemical*, vol. 208, pp. 122–127, 2015, doi: 10.1016/j.snb.2014.10.119.

[10] Y. Li, N. Chen, D. Deng, X. Xing, X. Xiao, and Y. Wang, "Formaldehyde detection: SnO2 microspheres for formaldehyde gas sensor with high sensitivity, fast response/recovery and good selectivity," *Sensors and Actuators B: Chemical*, vol. 238, pp. 264–273, 2017, doi: 10.1016/j.snb.2016.07.051.

[11] H. Du, P. J. Yao, Y. Sun, J. Wang, H. Wang, and N. Yu, "Electrospinning hetero-nanofibers In2O3/SnO2 of homotype heterojunction with high gas sensing activity," *Sensors (Switzerland)*, vol. 17, no. 8, p. 1822, 2017, doi: 10.3390/s17081822.

[12] M. A. Kadhim, A. A. Ramadhan, and M. O. S. Al-Gburi, "Effect of PEG addition on an SnO2 gas sensor fabricated using spin coating," *Karbala Int. J. Mod. Sci.*, vol. 7, no. 1, pp. 72–82, 2021, doi: 10.33640/2405-609X.2486.

[13] R. Kumar, X. Liu, J. Zhang, and M. Kumar, "Room-Temperature Gas Sensors Under Photoactivation: From Metal Oxides to 2D Materials," *Nano-Micro Lett.*, vol. 12, article no.: 164, pp. 1–37, 2020, doi: 10.1007/s40820-020-00503-4.

[14] M.C.Carotta, A.Cervi, A.Fioravanti, S.Gherardi, A.Giberti, B.Vendemiati, D.Vincenzi, M.Sacerdoti, "A novel ozone detection at room temperature through UV-LED-assisted ZnO thick film sensors," *Thin Solid Films*, vol. 520, no. 3, pp. 939–946, 2011, doi: 10.1016/j.tsf.2011.04.173.

[15] F. Li, T. Zhang, X. Gao, R. Wang, and B. Li, "Coaxial electrospinning heterojunction SnO2/ Au-doped In2O3 core-shell nanofibers for acetone gas sensor," *Sensors and Actuators B: Chemical*,

vol. 252, pp. 822–830, 2017, doi: 10.1016/j.snb.2017.06.077.
[16] W. H. Bragg and W. L. Bragg, *X Rays and Crystal Structure*. London: G. Bell and Sons, LTD., 1918.
[17] Y. F. Sun, S. B. Liu, and F. L. Meng, J.Y. Liu, Z. Jin, L.T.Kong, and J.H. Liu, "Metal oxide nanostructures and their gas sensing properties: A review," *Sensors(basel)*, vol. 12, no. 3, pp. 2610–2631, 2012, doi: 10.3390/s120302610.
[18] A. Umar, "Synthesis of donut-like SnO2 structures composed of small nanocrystals on silicon substrate: Growth mechanism , structural and optical properties," *J. Alloy. Compd.*, vol. 485, no. 1-2, pp. 759–763, 2009, doi: 10.1016/j.jallcom.2009.06.100.
[19] H. Ren, C. Gu, S. W. Joo, J. Cui, Y. Sun, and J. Huang, "Preparation of SnO2 nanorods on reduced graphene oxide and sensing properties of as-grown nanocomposites towards hydrogen at low working temperature," *Mater. Express*, vol. 8, no. 3, pp. 263–271, 2018, doi: 10.1166/mex.2018.1428.
[20] S. P. Mondal, S. K. Ray, J. Ravichandran, and I. Manna, "Temperature dependent growth and optical properties of SnO 2 nanowires and nanobelts," *Bull. Mater. Sci.*, vol. 33, no. 4, pp. 357–364, 2010, doi: 10.1007/s12034-010-0054-4.
[21] P. Feng, F. Shao, Y. Shi, and Q. Wan, "Gas sensors based on semiconducting nanowire field-effect transistors," *Sensors (Basel).*, vol. 14, no. 9, pp. 17406–17429, 2014, doi: 10.3390/s140917406.
[22] A. Das, S. K. Gautam, D. K. Shukla, and F. Singh, "Correlations of charge neutrality level with electronic structure and p-d hybridization," *scientific reports* , vol. 7, article no:40843, pp. 1–11, 2017, doi: 10.1038/srep40843.
[23] L.F.da Silva, J.-C.M'Peko, A.C.Catto, S. Bernardini, V. R.Mastelaro, K.Aguir, C.Ribeiro, E.Longo., " UV-enhanced ozone gas sensing response of ZnO-SnO 2 heterojunctions at room temperature," *Sensors and Actuators B: Chemical*, vol. 240, pp. 573–579, 2017, doi: 10.1016/j.snb.2016.08.158.
[24] T. Miyata, T. Hikosaka, and T. Minami, "Ozone gas sensors with high sensitivity using Zn2In2O5-MgIn2O4 multicomponent oxide thin films," *Surf. Coatings Technol.*, vol. 126, no. 2, pp. 219–224, 2000, doi: https://doi.org/10.1016/S0257-8972(00)00526-0.
[25] E. Espid and F. Taghipour, "UV-LED Photo-activated Chemical Gas Sensors : A Review," *critical reviews in Solid State Mateials Sciinces*, vol. 42, no. 5, pp. 416–432, 2017, doi: 10.1080/10408436.2016.1226161.
[26] S. Mills, M. Lim, B. Lee, and V. Misra, "Atomic Layer Deposition of SnO 2 for Selective Room Temperature Low ppb Level O3 Sensing," *ECS J. Solid State Sci. Technol.*, vol. 4, no. 10, pp. 3059–3061, 2015, doi: 10.1149/2.0111510jss..